

Resonant Raman scattering in GaAsN: Mixing, localization, and impurity band formation of electronic states

G. Bachelier, A. Mlayah, M. Cazayous, J. Groenen, and A. Zwick

Laboratoire de Physique des Solides UMR 5477, IRSAMC, Université P. Sabatier, 118 route de Narbonne, 31062 Toulouse Cedex 4, France

H. Carrère, E. Bedel-Pereira, and A. Arnoult

Laboratoire d'Analyse et d'Architecture des Systèmes UPR 8001, 7 Av. Du Colonel Roche, 31077 Toulouse, France

A. Rocher and A. Ponchet

Centre d'Elaboration de Matériaux et d'Etudes Structurales UPR 8011, 29 rue Jeanne Marvig, 31400 Toulouse, France

(Received 20 December 2002; published 30 May 2003)

Raman and TEM measurements on a thick GaAsN layer and on GaAsN/GaAs quantum well structures are reported. The scattering was excited close to resonance with the N-induced E_+ transition, and detected in both Stokes and anti-Stokes regions including the low-frequency range around the Rayleigh line. A broad continuous scattering due to acoustic phonons is observed on the thick GaAsN layer. Calculations of the Raman efficiency show that the localization and mixing of the resonant electronic states account well for the measured spectral line shapes. The localization length around a single nitrogen impurity is estimated and the impurity band formation discussed. Periodic oscillations of the scattered intensity are observed on the quantum well structures. They are analyzed in terms of Raman interference effects. The observed oscillations period, spectral envelope, and interference contrast are used to address the density distribution of the electronic states involved in the E_+ transition.

DOI: 10.1103/PhysRevB.67.205325

PACS number(s): 78.30.-j, 63.20.Kr, 81.07.Ta, 81.15.Hi

I. INTRODUCTION

The substitution of only 1% As atoms by N atoms in GaAs has important effects on the electronic and optical properties such as the giant band gap bowing,¹⁻³ the unusual pressure dependence of the band gap^{4,5} and large effective masses.^{6,7} Two models were proposed for the electronic structures of ternary alloys of highly mismatched binary semiconductors (e.g., GaN/GaP, GaN/GaAs, GaN/InAs). One is the band anticrossing (BAC) model,^{4,8,9} in which the electronic state of the isovalent impurity interacts strongly with the lowest conduction band states of the host material. The energies of the coupled electronic subbands, calculated using the BAC model, are in good agreement with the spectral features labeled E_- and E_+ revealed by modulated reflectance^{3,4} (PR) and photoluminescence⁵ measurements; the coupling strength was however used as an adjustable parameter. The BAC model is a phenomenological model since neither the origin of coupling nor the localization of the electronic states are considered explicitly. On the other hand Bellaïche *et al.*,¹⁰ Mattila *et al.*,¹¹ and Kent and Zunger^{12,13} reported calculations of the GaAsN and GaPN electronic structure using a pseudopotential supercell technique. The composition and pressure dependence of the lowest conduction band states were studied theoretically. It was shown that E_- and E_+ are due to transitions from the valence band maximum (VBM) to conduction states involving a strongly localized nitrogen state mixed with host crystal states arising from the Γ , L , and X valleys of the Brillouin zone. This approach well accounts for the PL and PR data as the BAC model does. But in addition to the transition energies, mixing

and localization of the electronic states come out as results of the calculations.¹¹⁻¹³

The aim of this work is to show that mixing and localization can be addressed directly using resonant Raman scattering by acoustic phonons. Indeed, THz acoustic phonons revealed by Raman scattering have been successfully used as probes of the electronic wave-function localization and correlation in quantum wells¹⁴⁻¹⁶ and quantum dot multilayers.^{17,18} In these systems, quantum confinement and artificial, as well as spontaneous, ordering are responsible for the spatial localization and correlation of the electronic density. In GaAsN, the localization of the electronic density around the nitrogen impurity originates in the large difference between the covalent radius of N (0.075 nm) and As (0.125 nm).

In this work we estimate the localization length of the resonantly excited electronic states using Raman scattering by acoustic phonons. Their degree of mixing is also discussed. The results are compared to previous calculations of the electronic structure performed using a pseudopotential supercell approach¹¹⁻¹³ and a large scale local density approximation.¹⁹ Moreover, the formation of an impurity band is addressed using interference Raman effects generated in GaAsN/GaAs multilayers. It is worth mentioning that, among the published Raman studies on GaAsN,²⁰⁻³¹ only a few were devoted to acoustic phonon scattering.^{22,29-31} In addition, only thick GaAsN layers were studied up to now. Interference Raman effects similar to those already observed on quantum dot layers^{17,18} are here reported for the GaAsN/GaAs quantum well structures.

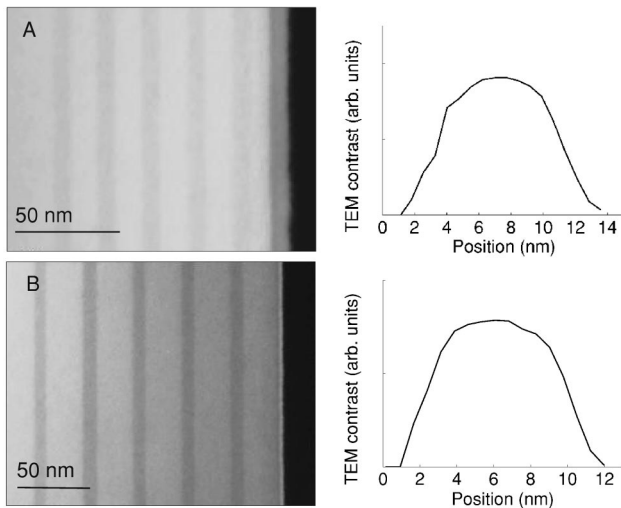


FIG. 1. 200 dark field images of samples A and B. The nitrogen profiles measured along the growth direction are shown for one of the quantum wells of structures A and B.

II. EXPERIMENTS

The samples studied in this work consist of a $1\text{-}\mu\text{m}$ -thick GaAsN layer and two GaAsN/GaAs quantum well structures grown by molecular beam epitaxy (MBE) on (100) GaAs. The MBE chamber is equipped with an Oxford Applied Research HD25R RF plasma cell, which provides reactive N species. Ultrapure N_2 was obtained from 6N nitrogen flowing through a heating getter filter to remove O_2 , H_2O , CO , CO_2 , and other impurities. The growth temperatures were 580 and 470 $^\circ\text{C}$ for the GaAs buffer layer and the GaAsN layer, respectively. Additional details of the growth conditions can be found elsewhere.³² The nitrogen composition was determined using secondary ion mass spectroscopy; a GaAsN layer previously characterized by x-ray diffraction was used as a reference. Cs^+ primary ions and CsM^+ positive secondary ions configuration was used in order to provide a quantitative analysis of nitrogen content up to few percents.

Figure 1 shows transmission electron microscopy (TEM) image of the quantum well structures under the 200 dark field conditions. Each structure consists of five GaAsN layers separated by GaAs spacers. The thickness of the GaAsN layers is about 9 nm for all structures whereas the barrier thickness is 12 or 24 nm. The GaAs top layer has the same thickness as the GaAs barriers.

For each structure the incorporation profile of the nitrogen along the growth direction was determined by a quantitative analysis of the TEM diffracted intensity.³³ The N composition, if lower than few percent, is proportional to the intensity ratio $[I_{200}(0) - I_{200}(N)]/I_0(0)$, where $I_{200}(0)$ and $I_{200}(N)$ are related to the GaAs barrier and the GaAsN well, respectively. For samples A and B, the nitrogen distribution inside the quantum wells is rather homogeneous (Fig. 1).

The Raman measurements were performed at liquid nitrogen temperature. The scattering was excited using the red and yellow lines of a Kr laser. The scattered light was dis-

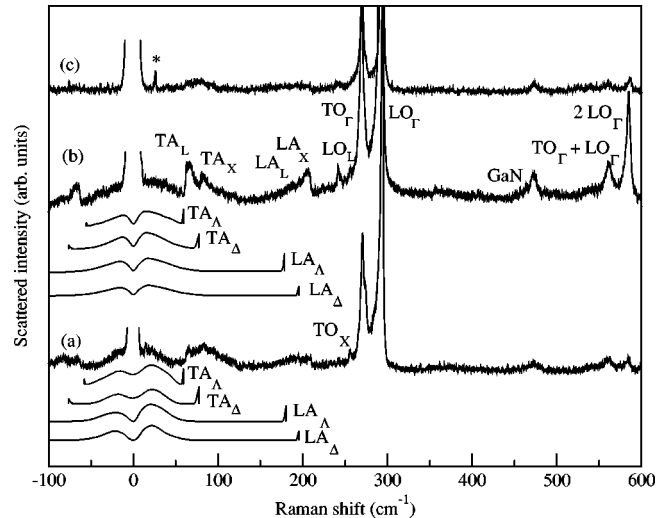


FIG. 2. Resonant Raman spectra from the $1\text{-}\mu\text{m}$ -thick $\text{GaAs}_{1-x}\text{N}_x$ layer for excitation at 1.83 eV (a), 1.91 eV (b), and 1.96 eV (c). The nitrogen composition is $x_{\text{SIMS}}=0.8\%$. Scaling factors were used in order to enable observation of the changes in the spectra. Calculated spectra show the activation of TA and LA phonons, in the Δ and Λ directions (ΓL and ΓX , respectively), due to wavefunction localization of the resonant state. The star in spectrum c indicates a plasma line.

persed using a triple T800 Coderg spectrometer and detected with a single channel GaAs photo-cathode.

III. RESULTS AND DISCUSSION

Figure 2 presents Stokes and anti-Stokes Raman spectra from the thick $\text{GaAs}_{1-x}\text{N}_x$ layer with $x_{\text{SIMS}}=0.8\%$. First and second order scattering by zone center transverse TO_Γ and longitudinal LO_Γ optical phonons of GaAs are observed. Scattering by the local vibrational mode (LVM) of isolated GaN bonds is also visible around 470 cm^{-1} . The dependence of the frequency and intensity of the TO_Γ , LO_Γ , and LVM lines, on the nitrogen composition, has been already studied in Refs. 21, 23, and 25. In particular, Prokofyeva *et al.*²¹ and Wagner *et al.*²³ showed that calibration of the frequency shift of the LO_Γ and LVM lines gives a reliable, rapid and non destructive method for determining the nitrogen content. Using the linear variations, as proposed by Prokofyeva *et al.*,²¹ and the measured frequency shifts, we obtain $x_{\text{LO}}=(0.8\% \pm 0.1\%)$ and $x_{\text{LVM}}=(0.9\% \pm 0.1\%)$ in good agreement with $x_{\text{SIMS}}=0.8\%$.

The spectra in Fig. 2 were excited close to resonance with the upper energy transition labeled E_+ and related to the nitrogen impurity. According to the electro-reflectance data of Perkins *et al.*³ we estimate E_+ about 1.86 eV (at liquid nitrogen temperature). As shown in Fig. 2, resonance occurs for excitation at 1.91 eV: first and second order scatterings by the GaAs zone center phonons TO_Γ and LO_Γ and by the GaN LVM strongly come out for excitation at 1.91 eV with respect to higher (1.96 eV) and lower (1.83 eV) energy.

Spectral features due to first order scattering by zone edge acoustic (TA_X , LA_X , TA_L , LA_L) and optical phonons (LO_L , TO_X) are clearly seen for resonant excitation. Such

scattering has been already observed by Cheong *et al.*²² and Seong *et al.*³¹ It is normally forbidden by the wave-vector conservation rule. Indeed, as long as the wave vector is a good quantum number, only zone-center phonon modes with wave vector $\mathbf{q}=(\mathbf{k}_i-\mathbf{k}_s)\sim\mathbf{0}$ can be detected (\mathbf{k}_i and \mathbf{k}_s being the wave vectors of the incident and scattered light, respectively). As a matter of fact, under excitation at 1.91 eV the Raman data from a GaAs reference sample showed no evidence for first order scattering by zone-edge phonons. Instead, second order scattering by zone-edge TA_L phonons is allowed and could be observed because of resonance with the indirect transition from the VBM to the conduction L point.

A. Wave-function localization

As already noted by Cheong *et al.*²² and Seong *et al.*,³¹ the observation of first order scattering by zone edge phonons is the signature of spatial localization of the resonant electronic states. Indeed, the Raman scattering is not a direct interaction between light and vibrations. It occurs via excitation and relaxation of electronic states. When these intermediate states become localized on a length scale l , the wave-vector conservation rule breaks down, and phonons with wave vectors up to $\sim\pi/l$ can be excited. The spatial distribution of the electronic density determines the spectral shape of the Raman scattering. In the frequency range of optical phonons, localization of the resonant electronic states lead only to asymmetric broadening of the Raman lines,²² because optical phonons have a relatively small frequency dispersion. In addition, their $1/q$ coupling to the electrons via Fröhlich interaction favors the Brillouin zone center.

The frequency dispersion of acoustic phonons is linear over a wide range of the Brillouin zone. Their interaction with electrons, via deformation potential, increases as q . So, one can look to the spectral distribution of the low-frequency Raman scattering as the image of the electronic density distribution in the reciprocal space.^{15–18} Conversely, one can extract the electronic density in real space from the acoustic phonon Raman spectra, allowing an efficient comparison with band structure calculations.

Calculations of the GaAsN electronic structure have been performed by Mattila *et al.*¹¹ and Kent and Zunger^{12,13} using a pseudopotential supercell technique. It was shown that E_+ and E_- are due to transitions from the VBM to conduction states consisting of mixed nitrogen impurity state $a_1(N)$ and host states $a_1(\Gamma)$, $a_1(L)$, and $a_1(X)$ associated with the center Γ and edge (L , X) points of the GaAs Brillouin zone. The degree of localization and mixing of these so-called perturbed host states (PHSs) depend on the nitrogen content: in the dilute impurity limit, E_+ involves a strongly localized nitrogen $a_1(N)$ state of which energy is inside the GaAs conduction band; this state, labeled $a_1(2)$, acquires Γ and L characters and shifts to higher energy with increasing nitrogen content.

For the nitrogen composition studied in Fig. 2 ($x_{\text{SIMS}}=0.8\%$) the percentage of Γ and L components is 30% and 61%, respectively. These values were calculated by Mattila *et al.*¹¹ using a spectral projection of the alloy states on the

GaAs Bloch states.³⁴ The probability for direct optical transitions from the VBM to the conduction band is proportional to the Γ component of the final state.⁴ For the E_+ transition, the conduction states retain about 30% of the Γ component, explaining the enhancement of the Raman efficiency at resonance with E_+ (Fig. 2). Moreover, 200 meV above $a_1(2)$ there is another mixed state labeled $a_1(3)$,^{12,13,19} which could also contribute to resonance. In fact, $a_1(3)$ has a majority of the X component (93%) and only 3% of the Γ component¹² at a nitrogen composition $x=0.8\%$. Therefore, the contribution to the resonance of the Raman scattering should be very weak in comparison with that of $a_1(2)$.

In Fig. 2 are presented Raman spectra calculated assuming a wave-function localization of the resonant electronic states and interaction with acoustic phonons via deformation potential mechanism.³⁵ Since we are interested in the activation of large wave-vector acoustic modes as well as zone-edge modes, we used a polynomial fit to the measured dispersion curves,³⁶ rather than the linear dispersion valid only for long-wavelength modes. Because of the three-dimensional localization of the electronic wave functions all orientations of the phonon wave vectors should be taken into account. However, since a mixing of electronic states involves mainly Γ , L , and X states, we have considered only the $[100]$ and $[111]$ crystallographic directions. Moreover, we disregarded possible localization of acoustic vibrations due to N-induced disorder effects.

We used a Gaussian function as a simple model for the electronic wave function localized on the nitrogen atom (isolated impurity); the localization length l is defined as the half width at half maximum of the electronic density distribution. Then, we considered the scattering due to an ensemble of spatially distributed localized states. We assumed a random distribution. Notice that such an assumption should be reconsidered in the case of the quaternary alloy GaInAsN, where short range order effects could lead to the formation of InN and GaAs bonds preferentially.³⁷

The ensemble wave function is constructed simply by a coherent superposition of localized states; the average distance d between neighboring impurities is about 1.6 nm for $x=0.8\%$. Hence, the electronic density could be either strongly localized with randomly distributed local maxima or totally uniform depending on the ratio l/d . The comparison between calculated and measured low-frequency Raman (Fig. 2) spectra shows the following:

First, the broad continuous scattering around the Rayleigh peak, and the sharp lines due to zone edge acoustic phonons, are both due to the activation of TA and LA acoustic phonons. The very low-frequency range (-50 – 50 cm^{-1}) corresponds to linear dispersion of the acoustic modes. Whereas the lines are due to nearly flat dispersion close to the Brillouin zone edges.

Second, the low frequency scattering is activated because of spatial localization of the resonant electronic states. The localization lengths $l=1.25$ and 1.7 nm were used in the calculations for excitation at 1.91 and 1.83 eV, respectively. These values give a good agreement between the calculated and measured spectral extents and line shape of the low-frequency scattering (Fig. 2). Different conduction states are

probed when changing the excitation energy. Our results indicate that the localization length increases when electronic states closer to the conduction band minimum (CBM) are selected. This is consistent with the calculations of Kent and Zunger,¹² who showed that above the limit of amalgamation between the nitrogen cluster states and perturbed host states ($x \geq 0.6\%$), there is a continuum of quasi-localized states within 0.4 eV above the CBM; the states close to the CBM are delocalized because of their large Γ component, whereas those around a CBM + 0.4 eV exhibit localization. According to Kent and Zunger¹² and Wang *et al.*¹⁹ nearly 80% of the electronic density is inside a sphere of 2-nm radius and centered at the N impurity. From our estimate of the localization lengths l this percentage is about 69% and 41% for excitations at 1.91 and 1.83 eV, respectively.

Third, TA_X , LA_X , TA_L , and LA_L lines come out strongly in the measured spectra (spectrum *b* of Fig. 2): their calculated intensity is underestimated with respect to the intensity of the broadband scattering. This is certainly due to the lack of zone-edge components of the localized electronic state. In fact, we did not take into account explicitly the mixing between Γ , L , and X states. In that way, one could estimate the amount of zone-edge components (i.e., mixing) to be added to the Gaussian wave-function in order to fit the experimental spectra (Fig. 2). The comparison with the experimental data (spectrum excited at 1.91 eV) indicates that mixing of Γ , L , and X states is indeed relevant as already pointed out by Cheong *et al.*²² and Seong *et al.*³¹ Notice that the spectrum measured at 1.83 eV compares rather well with the calculated spectra: zone-edge features and broadband scattering have similar intensities. This means that the electronic conduction states selected by excitation at 1.83 eV have a majority of the Γ component. This is consistent with the larger localization length 1.7 nm (instead of 1.25 nm for excitation at 1.91 eV).

B. Impurity band formation

It is interesting to compare the localization length l of the electronic state around a single nitrogen impurity and the average distance d (1.6 nm) between nearest neighbor impurities: our estimations show that $l \approx d$, and indicate the formation of an impurity band (at a nitrogen content $x = 0.8\%$). The calculations based on the pseudopotential method showed no evidence for the formation of an impurity band of cluster states (CSs). These states are located in the band gap and are strongly localized explaining the weak CS-CS interaction and the absence of an impurity band.¹² In comparison of the CS, the PHSs are less localized states and their wave functions spread over distance which could be comparable to the average separation between impurities.^{12,13,19} In our calculations of the Raman spectra, the formation of an impurity band was not taken into account explicitly since interaction between quasilocated states was ignored. However, we used an ensemble wave function which is one of the impurity band eigenstates (i.e., the one with no dephasing between the distributed states). The present model for resonant Raman scattering is thus more

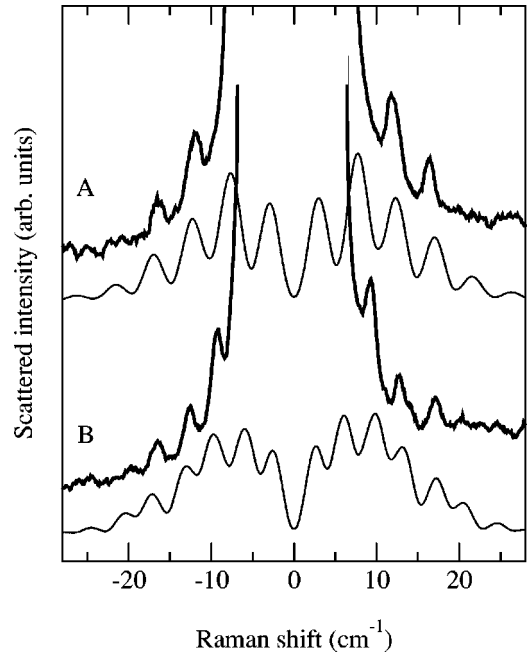


FIG. 3. Calculated (thin lines) and measured (bold lines) Raman spectra of the GaAsN/GaAs quantum well structures. Optical excitation has been performed at 1.91 eV close to resonance with E_+ . The thicknesses of the GaAs spacers are 12 and 24 nm for samples A and B, respectively.

realistic than the one in which only a single (average) state was assumed.²⁹ Further evidence for the formation of an impurity band is given by the Raman interference effects.

Raman scattering by acoustic vibrations is a spatially coherent process, and this leads to interference effects in the Raman efficiency: the emission and absorption rates of a given vibrational mode could be either enhanced or inhibited depending on the spatial distribution of the resonantly excited electronic density. As already shown for quantum wells¹⁴⁻¹⁶ and quantum dot multilayers,^{17,18} strong oscillations of the Raman spectra could be observed in the acoustic phonons frequency range. The intensity maxima correspond to bright fringes and the minima to dark fringes. The interference, the interference contrast, and the spectral envelope of the oscillations are determined by the electronic density distribution in the sample.¹⁸

Periodic oscillations of the low-frequency Raman spectra are clearly observed for both samples A and B (Fig. 3). They originate from the interference between the Raman scattering amplitudes associated with each GaAsN quantum well and are observed only for resonant excitation (with the E_+ transition). The non-resonant spectra are very similar to the one shown in Fig. 2(c), where no signature of the nitrogen impurities was detected. The period of the Raman fringes is determined by the sound velocity and by the separation between quantum wells. Their relative intensities (spectral envelope) is a form factor given by the Fourier transform of the electronic density distribution in each quantum well. The interference contrast is directly connected to the interlayer correlation of the electronic density.^{17,18}

The same scattering model as the one discussed for the thick GaAsN layer has been used to calculate the Raman

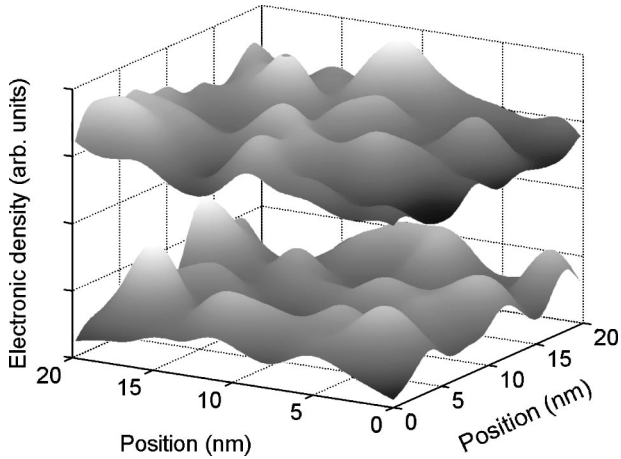


FIG. 4. In-plane electron density distribution (cross section) used for the calculations of the resonant Raman spectra. It is shown only for two GaAsN/GaAs quantum wells, and was generated assuming a coherent superposition of randomly distributed localized states centered on the nitrogen impurities.

spectra shown in Fig. 3. Reflection of the sound waves at the sample surface was taken into account.^{38,39} The main difference from the spectra in Fig. 2 is the spatial distribution of the resonant electronic wave function. Instead of the three-dimensional distribution of impurities, now we have a layering of the wave function along the growth direction. Since the energy of the resonant $a_1(2)$ state is above the GaAs CBM, quantum confinement effects are not expected.

According to the growth conditions the nitrogen composition in the quantum wells should be the same as in the thick GaAsN layer. So, we used an ensemble wave function of randomly distributed nitrogen impurities in each GaAsN quantum wells with the parameters l and d obtained from the thick GaAsN layer.

Figure 4 shows the in-plane electronic density in two of the five GaAsN/GaAs quantum wells used for the calculations. The parameters, such as the thickness of the quantum wells and distance between the quantum wells, were taken from the TEM images in Fig. 1. As one can see in Fig. 3, a good agreement between calculated and measured spectra is obtained for samples A and B. The period and spectral envelope of the oscillations as well as the interference contrast are well accounted for. In order to appreciate the sensitivity of the interference contrast to the localization of the electronic wave function, calculations were performed for constant l and various values of d (i.e., of nitrogen concentration). As shown in Fig. 5 clear periodic oscillations (maximum contrast) come out for a quasiuniform electronic density distribution in the plane of the quantum wells ($d=l/5$), whereas strongly localized and isolated states ($d=5l$) lead to a continuous scattering (vanishing contrast). The parameter l extracted from the thick GaAsN layer gives a good agreement between calculated and observed interference contrasts (Fig. 3) for a 0.8% nitrogen concentration in the quantum wells. The measured strong interference contrast is consistent with

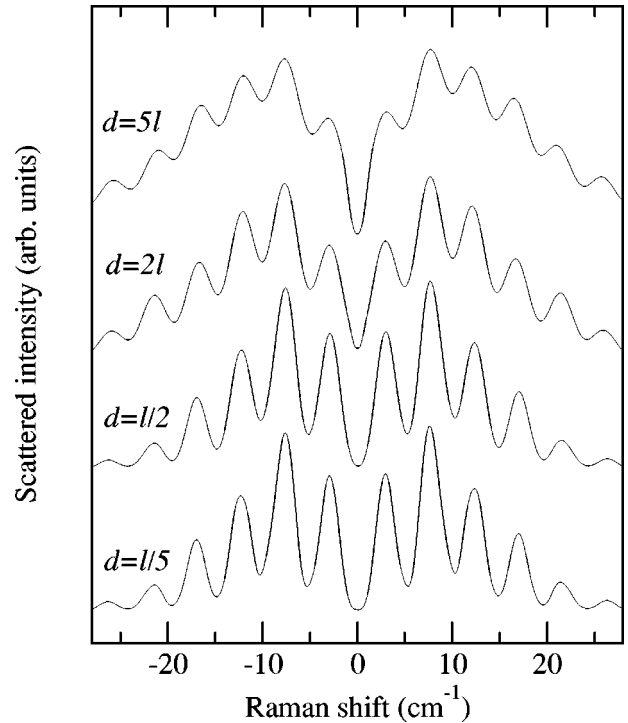


FIG. 5. Calculated Raman spectra for a fixed localization length l of the electronic density around an isolated nitrogen impurity and for various mean distances d between nearest neighbor impurities. Calculations were performed assuming statistical random distributions of the nitrogen inside the quantum wells. The width of the quantum wells and the separation between quantum wells are those measured for sample A.

the formation of an impurity band: for the studied nitrogen content, the E_+ transition involves quasi-delocalized states arising from the overlap of the wavefunctions located at neighboring nitrogen impurities.

IV. CONCLUSION

Resonant Raman scattering, detected in the frequency range of acoustic phonons, reveals the spatial distribution of the excited electronic density. We have applied this approach to the study of electronic wave-function localization in GaAsN. Our main findings can be summarized as follows. (i) By comparing calculated and measured Raman spectra we have extracted the localization length of the conduction states involved in the E_+ optical transition. We have found a good agreement with the electronic structure predicted by the pseudopotential supercell method and by the large scale local density approximation. (ii) Impurity band formation has been addressed using an ensemble wave function for the calculations of the Raman spectra. (iii) Interference Raman effects have been generated by layering the electronic density along one direction (multiple quantum wells). We have observed a strong interference contrast on the quantum well structures. This supports partial delocalization of the electronic density over many nitrogen impurities, i.e., the formation of an impurity band at the studied nitrogen concentration.

- ¹ M. Weyers, M. Sato, and H. Ando, *Jpn. J. Appl. Phys.* **31**, L853 (1992).
- ² J. Salzman and H. Temkin, *Mater. Sci. Eng., B* **50**, 148 (1997).
- ³ J. D. Perkins, A. Mascarenhas, Yong Zhang, J. F. Geisz, D. J. Friedman, J. M. Olson, and Sarah R. Kurtz, *Phys. Rev. Lett.* **82**, 3312 (1999).
- ⁴ W. Shan, W. Walukiewicz, J. W. Ager III, E. E. Haller, J. F. Geisz, D. J. Friedman, J. M. Olson, and S. R. Kurtz, *Phys. Rev. Lett.* **82**, 1221 (1999).
- ⁵ E. D. Jones, N. A. Modine, A. A. Allerman, S. R. Kurtz, A. F. Wright, S. T. Tozer, and X. Wei, *Phys. Rev. B* **60**, 4430 (1999).
- ⁶ Y. Zhang, A. Mascarenhas, H. P. Xin, and C. W. Tu, *Phys. Rev. B* **61**, 7479 (2000).
- ⁷ C. Skierbiszewski, P. Perlin, P. Wisniewski, W. Knap, T. Suski, W. Walukiewicz, W. Shan, K. M. Yu, J. W. Ager, E. E. Haller, J. F. Geisz, and J. M. Olson, *Appl. Phys. Lett.* **76**, 2409 (2000).
- ⁸ W. Shan, W. Walukiewicz, K. M. Yu, J. Wu, J. W. Ager III, E. E. Haller, H. P. Xin, and C. W. Tu, *Appl. Phys. Lett.* **76**, 3251 (2000).
- ⁹ W. Walukiewicz, W. Shan, K. M. Yu, J. W. Ager III, E. E. Haller, I. Miotkowski, M. J. Seong, H. Alawadhi, and A. K. Ramdas, *Phys. Rev. Lett.* **85**, 1552 (2000).
- ¹⁰ L. Bellaiche, Su-Huai Wei, and A. Zunger, *Phys. Rev. B* **54**, 17568 (1996).
- ¹¹ T. Mattila, Su-Huai Wei, and A. Zunger, *Phys. Rev. B* **60**, R11245 (1999).
- ¹² P. R. C. Kent and A. Zunger, *Phys. Rev. Lett.* **86**, 2613 (2001).
- ¹³ P. R. C. Kent and A. Zunger, *Phys. Rev. B* **64**, 115 208 (2001).
- ¹⁴ T. Ruf, in *Phonon Raman Scattering in Quantum Wells and Superlattices*, edited by G. Höhler (Springer, Berlin, 1998), Vol. 142.
- ¹⁵ V. F. Sapega, V. I. Belitsky, A. J. Shields, T. Ruf, M. Cardona, and K. Ploog, *Solid State Commun.* **84**, 1039 (1992).
- ¹⁶ A. Mlayah, R. Grac, G. Armelles, R. Carles, A. Zwick, and F. Briones, *Phys. Rev. Lett.* **78**, 4119 (1997).
- ¹⁷ M. Cazayous, J. R. Huntzinger, J. Groenen, A. Mlayah, S. Christiansen, H. P. Strunk, O. G. Schmidt, and K. Eberl, *Phys. Rev. B* **62**, 7243 (2000).
- ¹⁸ M. Cazayous, J. Groenen, J. R. Huntzinger, A. Mlayah, and O. G. Schmidt, *Phys. Rev. B* **64**, 033306 (2001).
- ¹⁹ Lin.-Wang Wang, *Appl. Phys. Lett.* **78**, 1565 (2001).
- ²⁰ A. M. Mintairov, P. A. Blagnov, V. G. Melehin, N. N. Faleev, J. L. Merz, Y. Qiu, S. A. Nikishin, and H. Temkin, *Phys. Rev. B* **56**, 15836 (1997).
- ²¹ T. Prokofyeva, T. Sauncy, M. Seon, M. Holtz, Y. Qiu, S. Nikishin, and H. Temkin, *Appl. Phys. Lett.* **73**, 1409 (1998).
- ²² H. M. Cheong, Y. Zhang, A. Mascarenhas, and J. F. Geisz, *Phys. Rev. B* **61**, 13687 (2000).
- ²³ J. Wagner, K. Khler, P. Ganser, and N. Herres, *Appl. Phys. Lett.* **77**, 3592 (2000).
- ²⁴ Yong Zhang, A. Mascarenhas, J. F. Geisz, H. P. Xin, and C. W. Tu, *Phys. Rev. B* **63**, 085205 (2001).
- ²⁵ M. J. Seong, M. C. Hanna, and A. Mascarenhas, *Appl. Phys. Lett.* **79**, 3974 (2001).
- ²⁶ A. Hashimoto, T. Furuhashi, T. Kitano, A. K. Nguyen, A. Masuda, and A. Yamamoto, *J. Cryst. Growth* **227**, 532 (2001).
- ²⁷ J. Wagner, T. Geppert, K. Khler, P. Ganser, and N. Herres, *J. Appl. Phys.* **90**, 5027 (2001).
- ²⁸ T. Geppert, J. Wagner, K. Khler, P. Ganser, and M. Maier, *Appl. Phys. Lett.* **80**, 2081 (2002).
- ²⁹ G. Bachelier, A. Mlayah, A. Zwick, R. Carles, M. Cazayous, J. Groenen, H. Carrè, A. Arnoult, and E. Bedel, in *Proceedings of the International Conference on the Physics of Semiconductors, 2002, Edinburgh*.
- ³⁰ A. Mascarenhas and M.J. Seong, in *Proceedings of the International Conference on the Physics of Semiconductors, 2002, Edinburgh*.
- ³¹ M. J. Seong, A. Mascarenhas, and J. F. Geisz, *Appl. Phys. Lett.* **79**, 1297 (2001).
- ³² H. Carrère, A. Arnoult, A. Ricard, and E. Bedel-Pereira, *J. Cryst. Growth* **243**, 295 (2002).
- ³³ B. Piaud, A. Rocher, and A. Ponchet, Master Report, Université Paul Sabatier, Toulouse (2002).
- ³⁴ L. W. Wang, L. Bellaiche, S. H. Wei, and A. Zunger, *Phys. Rev. Lett.* **80**, 4725 (1998).
- ³⁵ B. Jusserand and M. Cardona, in *Light Scattering in Solids* (Springer, Berlin, 1979), Vol. 66.
- ³⁶ H. Bilz and W. Kreiss, in *Phonon Dispersion Relations in Insulators*, edited by M. Cardona, P. Fulde, and H. J. Queisser (Springer, Berlin, 1979).
- ³⁷ K. Kim and A. Zunger, *Phys. Rev. Lett.* **86**, 2609 (2001).
- ³⁸ J. R. Huntzinger, J. Groenen, M. Cazayous, A. Mlayah, N. Bertru, C. Paranthoen, O. Dehaese, H. Carrère, E. Bedel, and G. Armelles, *Phys. Rev. B* **61**, R10547 (2000).
- ³⁹ M. Cazayous, J. Groenen, A. Zwick, A. Mlayah, R. Carles, J. L. Bischoff, and D. Dentel, *Phys. Rev. B* **66**, 195320 (2002).